Supporting Information for

ORIGINAL ARTICLE

A tactical nanomissile mobilizing antitumor immunity enables neoadjuvant chemo-immunotherapy to minimize postsurgical tumor metastasis and recurrence

Tao He, Mingxing Hu, Shunyao Zhu, Meiling Shen, Xiaorong Kou, Xiuqi Liang, Lu Li, Xinchao Li, Miaomiao Zhang, Qinjie Wu*, Changyang Gong*

State Key Laboratory of Biotherapy and Cancer Center, West China Hospital, Sichuan University, Chengdu, 610041, China

Received 6 April 2022; received in revised form 7 Jun 2022; accepted 19 Jun 2022

*Corresponding authors. Tel./fax: +86 13541158521 (Changyang Gong), +86 13402823774 (Qinjie Wu).

E-mail addresses: chygong14@163.com (Changyang Gong), cellwqj@163.com (Qinjie Wu).

Table S1 List of antibodies applied to flow cytometric analysis.

Antibody	Clone	Fluorophore	Source
CD3	17A2	PE/Cyanine 7	Biolegend
CD4	GK1.5	PE	Biolegend
CD4	GK1.5	FITC	Biolegend
CD8α	53-6.7	FITC	Biolegend
CD8α	53-6.7	PE/Cyanine 7	Biolegend
CD11c	N418	PE	Biolegend
LRP1	EPR3724	Alexa Fluor® 488	Abcam
CD103	2E7	APC	Biolegend
CD4	RM4-5	FITC	eBioscience
CD25	PC61.5	PE	eBioscience
Foxp3	FJK-16s	PE/Cyanine 5	eBioscience
CD16/32 (Fc Block)	93	--	eBioscience
CD44	IM7	PE	Biolegend
CD62L	MEL-14	APC	Biolegend
HMGB1	--	FITC	Bioss

Table S2 Preparation of MAL with different AZO molar ratios.

	Ratio 1		Ratio 2		Ratio 3		Ratio 4		Ratio 5	
AZO	50%		60%		70%		80%		90%	
Cholesterol	45%		35%		25%		15%		5%	
DSPE-mPEG$_{2k}$	5%		5%		5%		5%		5%	
EE (%)	76.9		64.4		48.4		14.0		7.8	
DL (%)	8.0		7.3		4.9		1.2		0.9	
Days	0	7	0	7	0	7	0	7	0	7
Size (nm)	92.4	114.3	91.2	94.5	94.6	129.5	90.6	85.1	47.2	48.7
PDI	0.05	0.24	0.08	0.10	0.09	0.24	0.17	0.20	0.24	0.32

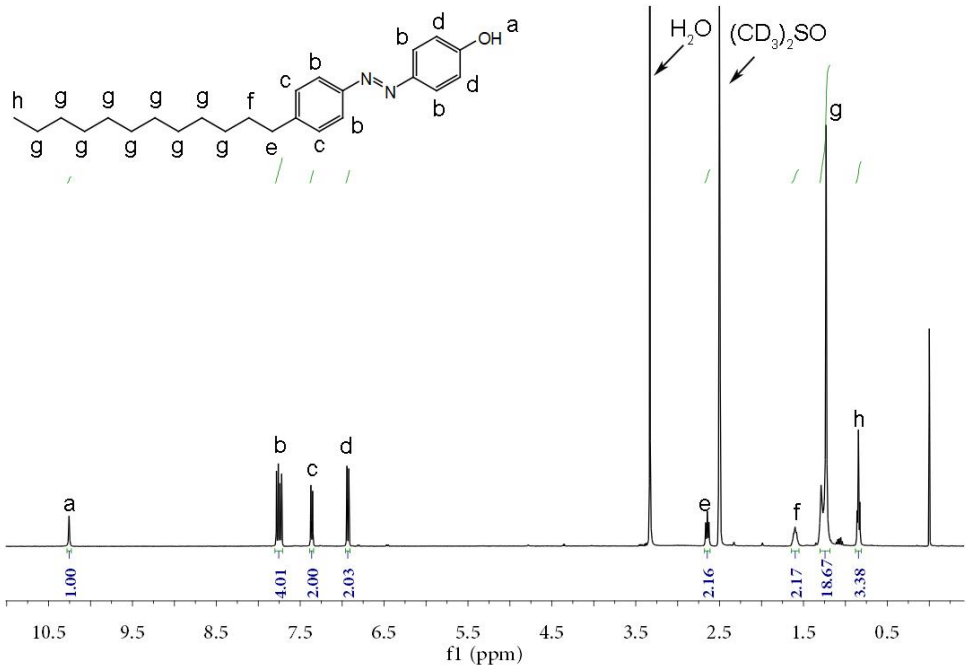

Figure S1 ^{1}H NMR spectra of compound A.

Figure S2 ^{1}H NMR spectra of compound B.

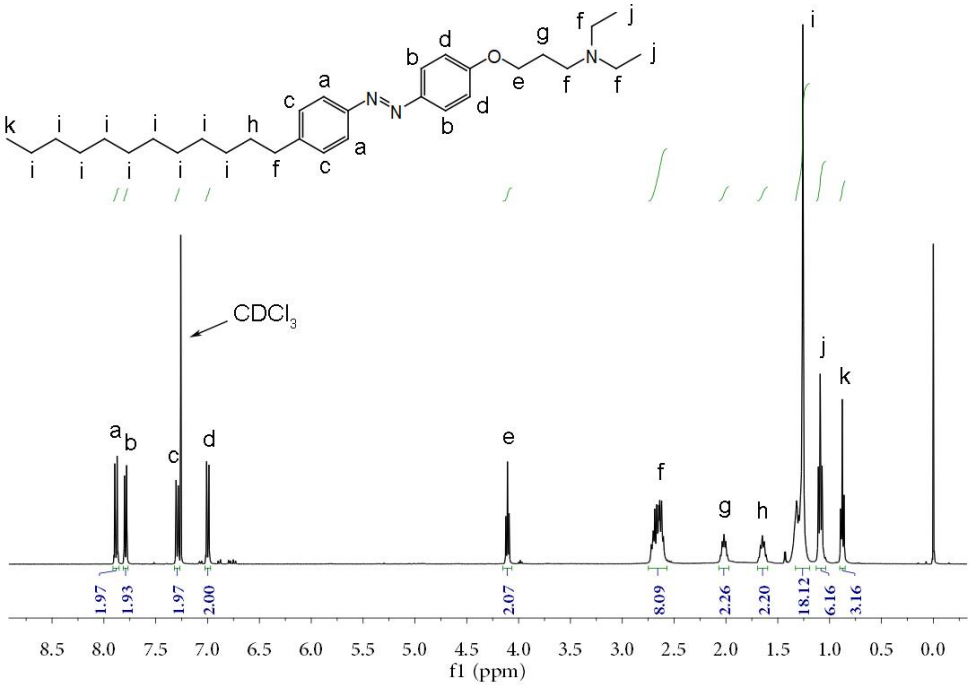

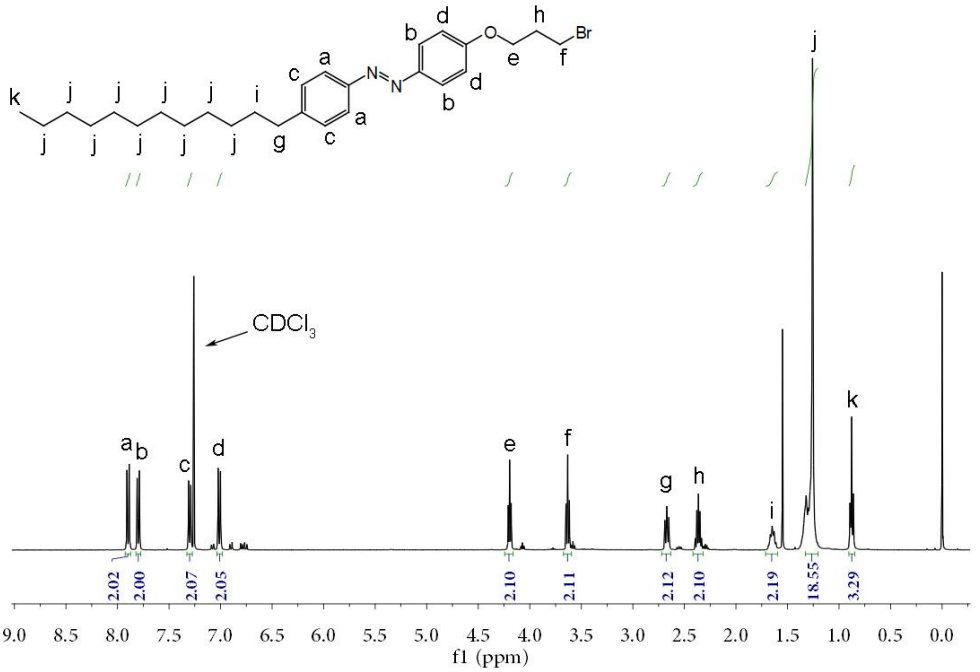

Figure S3 ^{1}H NMR spectra of AZO.

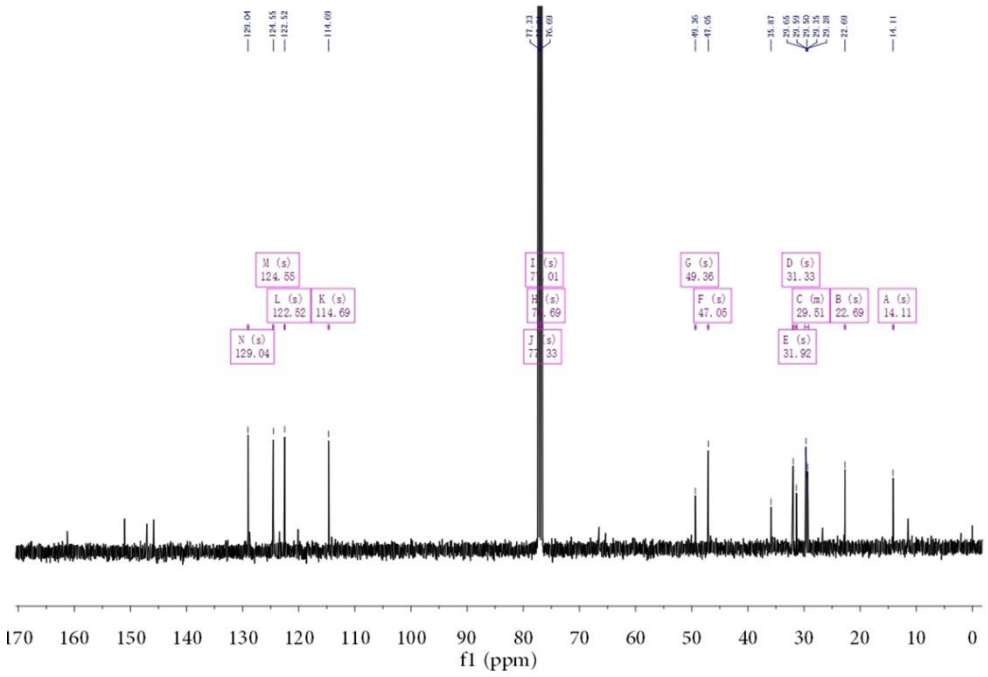

Figure S4 ^{13}C NMR spectra of AZO.

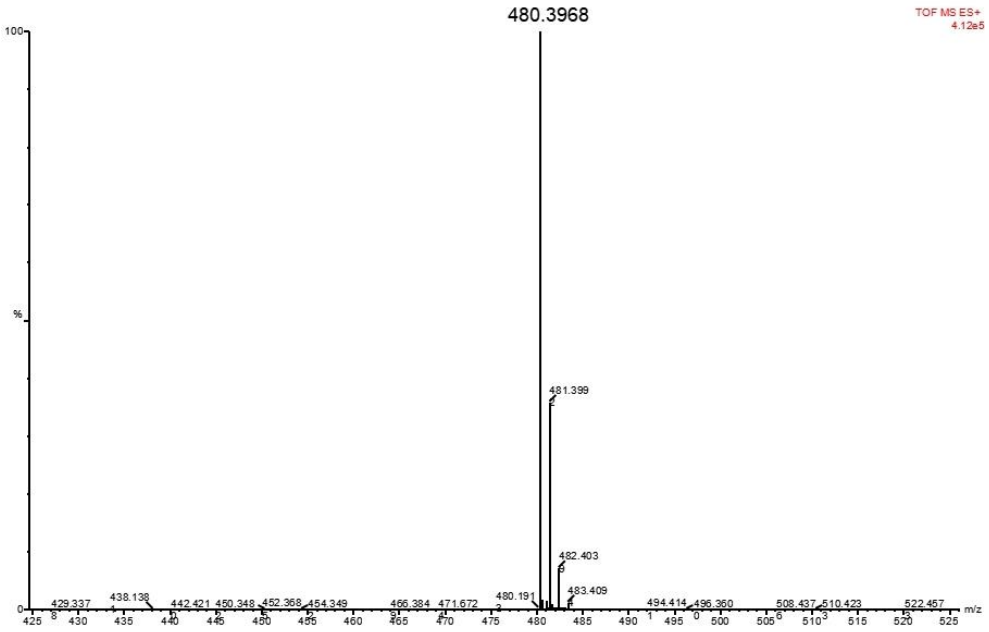

Figure S5 ESI-MS spectra of AZO.

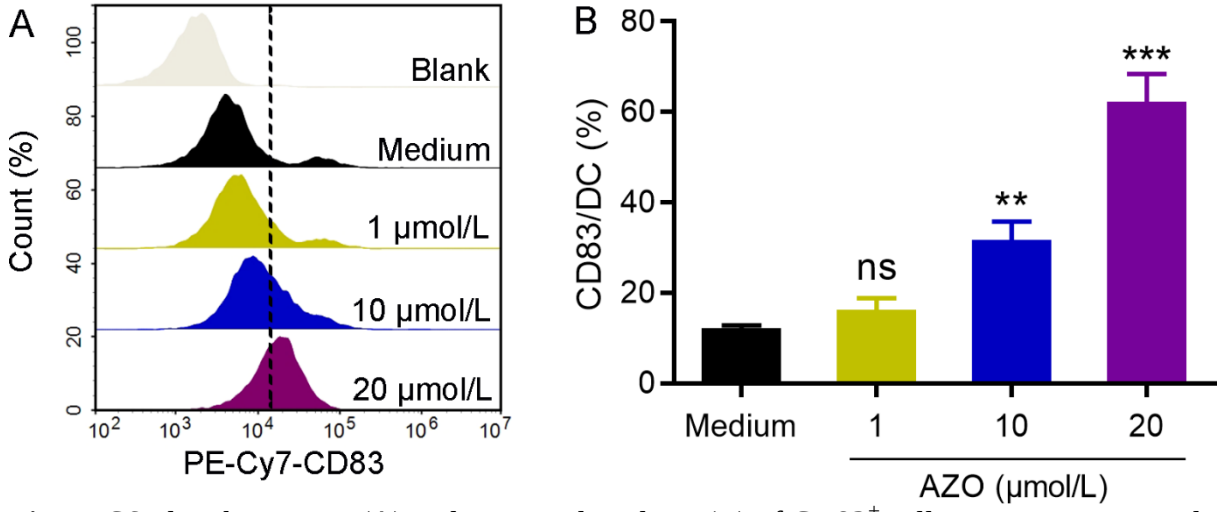

Figure S6 Flow histogram (A) and statistical analysis (B) of $CD83^+$ cells. Data are presented as mean±SD (n = 3). ***P<0.001, **P<0.01 indicate the statistical difference between each group and the Medium group, ns: not significant.

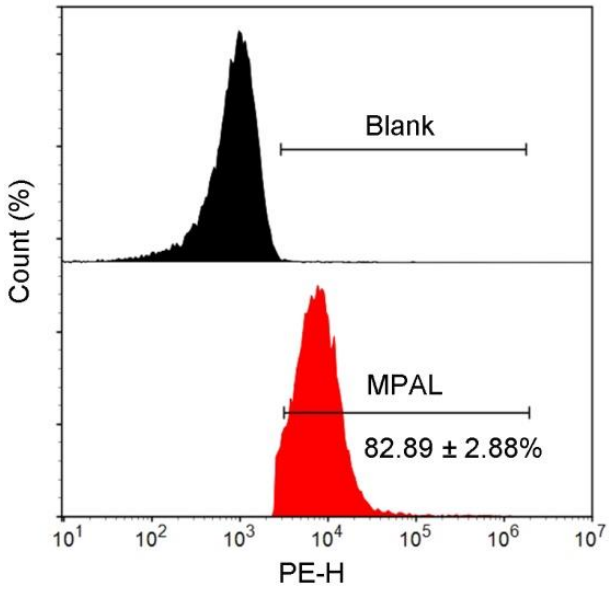

Figure S7 Flow cytometric examination of the insertion efficiency of aPD-L1 on MPAL.

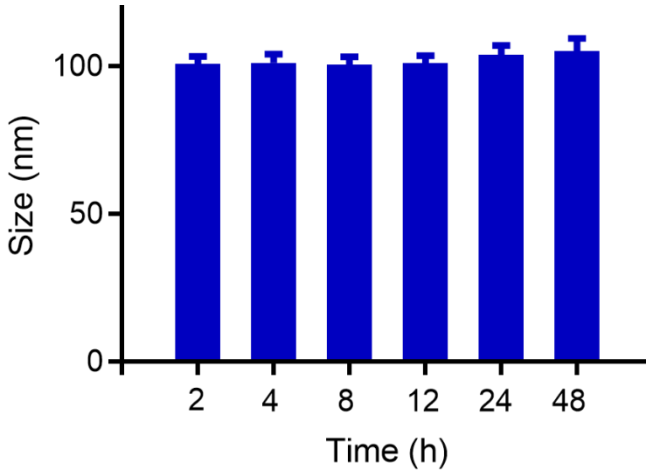

Figure S8 Size change of MPAL incubated in 50% FBS for 48 h. Data are presented as mean±SD (*n* = 3).

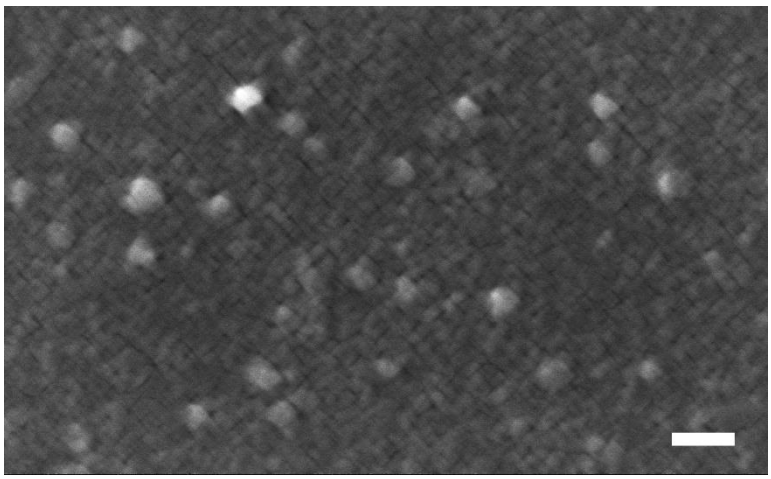

Figure S9 The FESEM image of MPAL (Scale bar: 200 nm).

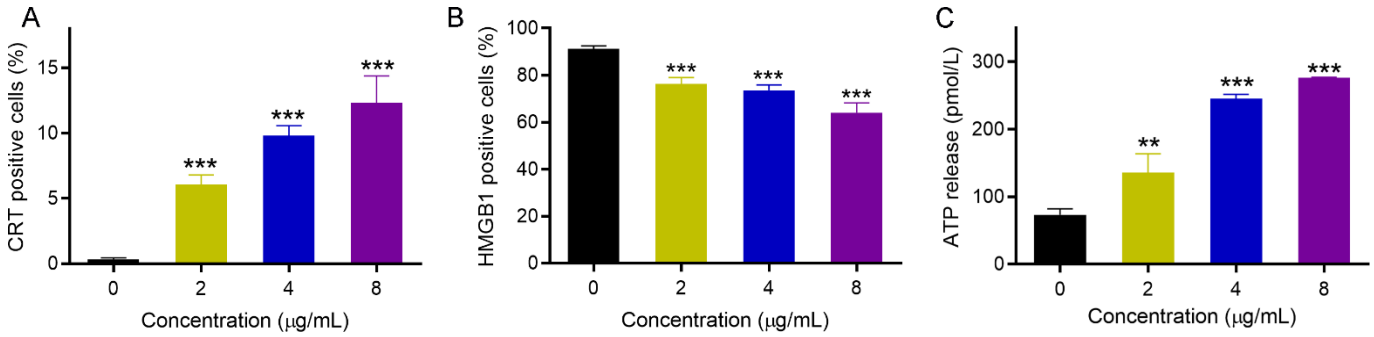

Figure S10 MPAL elicited the immunogenic death of B16-F10 cells. (A) CRT detections on B16-F10 cells after treated with different concentrations of MPAL using flow cytometry. (B) HMGB1 detections in B16-F10 cells after treated with different concentrations of MPAL using flow cytometry. (C) ATP production by B16-F10 cells after MPAL treatment. Data are presented as mean±SD (n = 3). ****P*<0.001 and ***P*<0.01 indicate the statistical difference between each group and the group without MPAL.

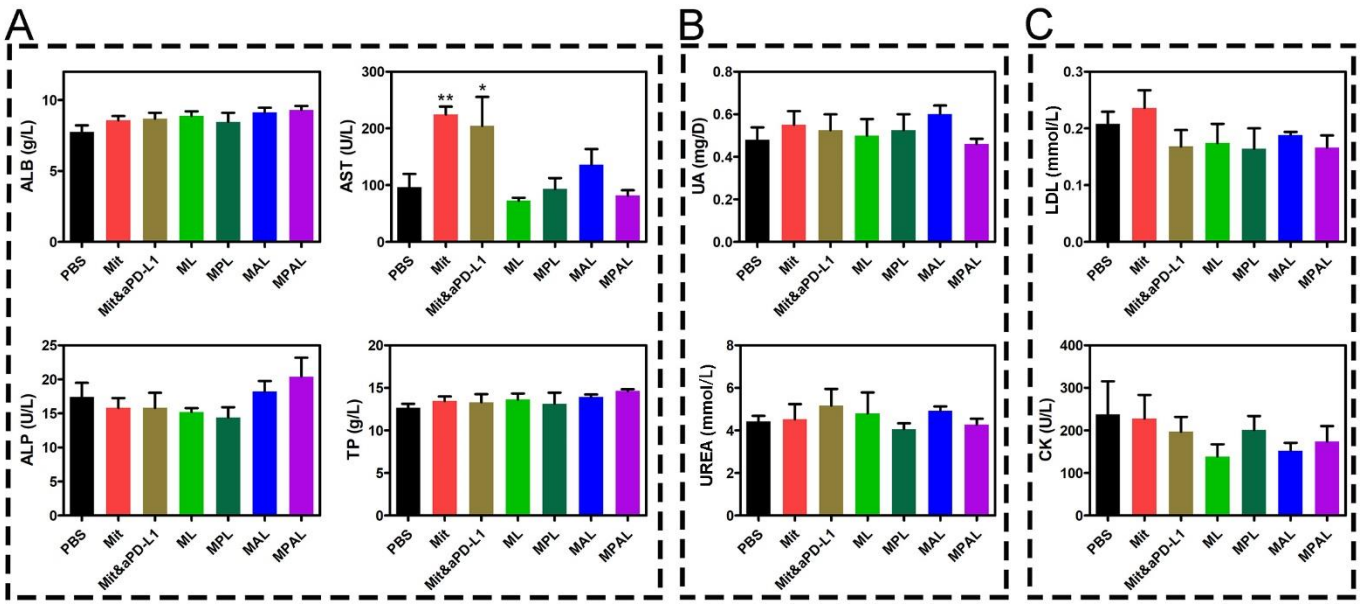

Figure S11 Blood chemistry profile of (A) liver, (B) kidney, and (C) heart functions-related indexes of mice in each group after treatment. Data are presented as mean±SD (*n*=3). **P*<0.05 and ***P*<0.01 indicate the statistical difference between each group and the PBS group.

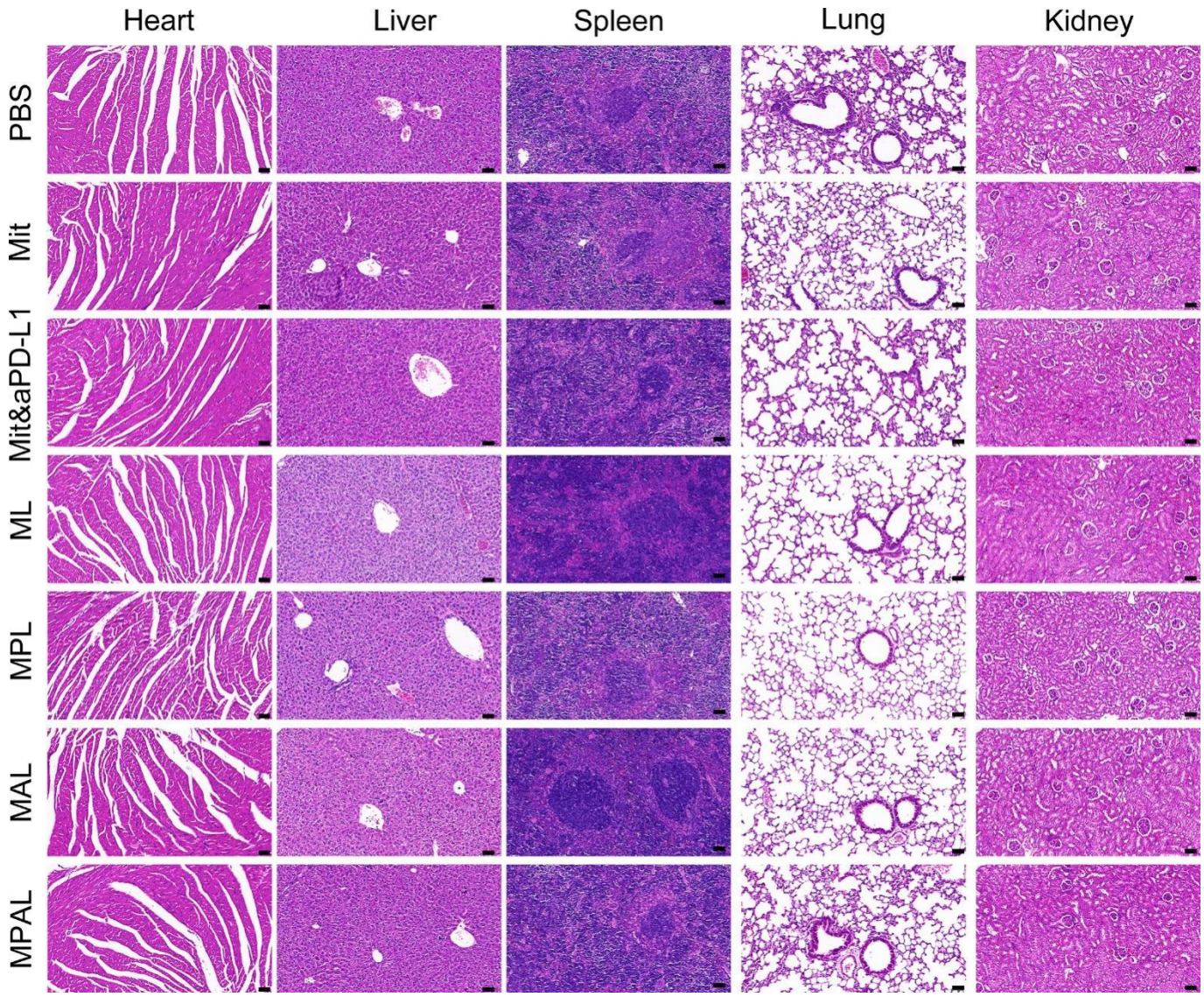

Figure S12 H&E staining of major organs in B16-F10 subcutaneous xenograft model after different treatments. (Scale bar: 50 μm).

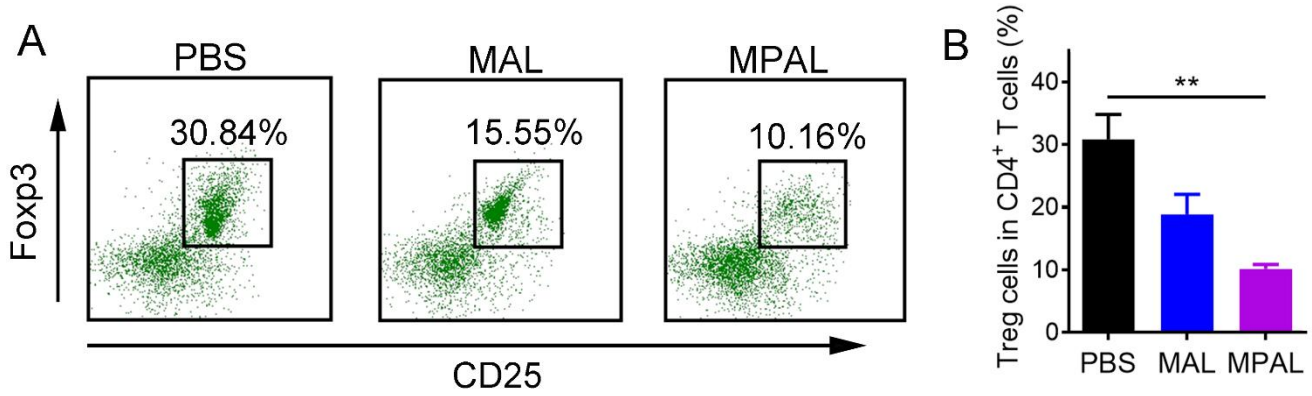

Figure S13 Flow scatter diagram of Treg ($CD3^+CD4^+CD25^+Foxp3^+$) (A) and its statistical analysis (B) in tumors. Data are presented as mean±SD (n = 3). $^{**}P<0.01$.

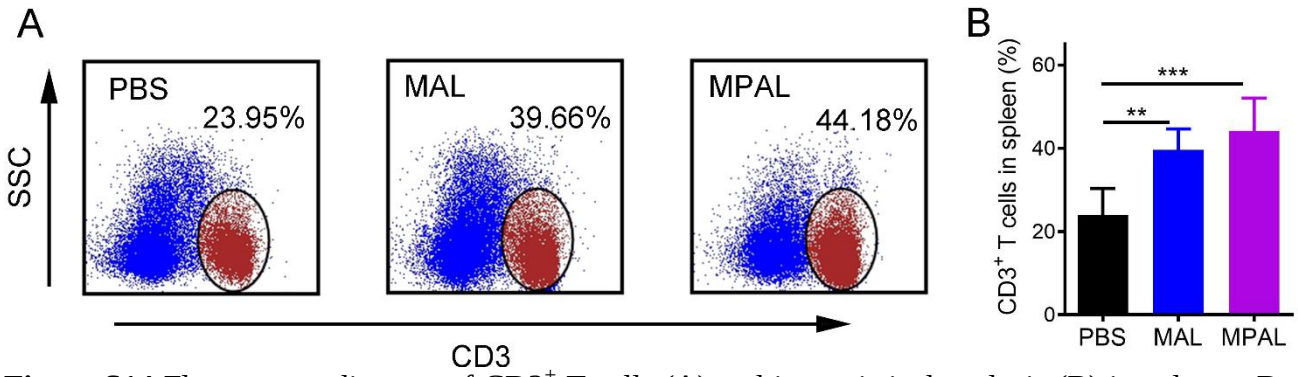

Figure S14 Flow scatter diagram of $CD3^+$ T cells (A) and its statistical analysis (B) in spleens. Data are presented as mean±SD (n = 3). $^{***}P<0.001$, $^{**}P<0.01$.